J. Fluid Mech. (1994), *vol.* 275, *pp.* 285–299

Surface-wave damping in a circular cylinder with a fixed contact line

By D. M. HENDERSON[1] AND J. W. MILES[2]

[1] Department of Mathematics, Pennsylvania State University, University Park, PA 16802, USA

[2] Institute of Geophysics and Planetary Physics, University of California, San Diego, La Jolla, CA 92093-0225, USA

(Received 3 January 1994 and in revised form 5 April 1994)

The natural frequencies and damping ratios for surface waves in a circular cylinder are calculated on the assumptions of a fixed contact line, Stokes boundary layers, and either a clean or a fully contaminated surface. These theoretical predictions are compared with the measurements for the first six modes in a brimfull, sharp-edged cylinder of radius 2.77 cm and depth 3.80 cm. The differences between the predicted and observed frequencies were less than 0.5 % for all but the fundamental axisymmetric mode with a clean surface. The difference between the predicted and observed damping ratio for the dominant mode with a clean surface was 20 %; this difference was significantly larger for the higher modes with a clean surface and for all of the modes with a contaminated surface.

1. Introduction

The damping of surface waves in a closed basin, which almost always exceeds theoretical predictions, is due to: (i) viscous dissipation at the rigid boundary of the basin, (ii) viscous dissipation at the (upper) surface, which may be covered by a viscoelastic film, (iii) viscous damping in the interior fluid, and (iv) capillary hysteresis at the contact line. The interior damping (iii) is negligible for water in a basin of lateral dimensions comparable with the wavelength, and we do not consider it further. We also assume that the motion is of sufficiently small wavelength to render damping in the aerodynamic boundary layer negligible (cf. Dore 1978) and of sufficiently small amplitude to ensure laminar flow.

The calculation of laminar damping at a rigid boundary goes back to Stokes (1851), who calculated the flow over an oscillating plane and remarked that the corresponding flow over a curved boundary 'may be calculated to a very close degree of approximation by regarding each element of the [boundary] as an element of an infinite plane oscillating with the same velocity'. It is implicit in this approximation that the minimum radius of curvature of the boundary must be large compared with the viscous length

$$l_\nu \equiv (2\nu/\omega)^{1/2} \tag{1.1}$$

(ν = kinematic viscosity, ω = angular frequency), which is 0.6 mm for a one-second wave on clean water.

The observation that surfactants, such as oil on water, can lead to appreciable damping of surface waves goes back to antiquity (see Scott 1977 for a historical survey). The physiochemical problem (see Miles 1967 for a brief review) depends on a large family of parameters, at least some of which have not been measured in the

spectral domain of gravity–capillary waves. However, both the dissipative and dispersive effects of a surface film on a wave of small amplitude are captured by the phenomenological boundary condition (Miles 1991*b*)

$$\boldsymbol{u}+l_S(\boldsymbol{u}_z+\boldsymbol{\nabla}w)=0, \tag{1.2}$$

where $\boldsymbol{u}$ is the horizontal velocity at the interface ($z=0$) between the film and the underlying liquid, $\boldsymbol{u}_z$ is the vertical gradient of $\boldsymbol{u}$, $\boldsymbol{\nabla}w$ is the horizontal gradient of the vertical velocity, and l_S is a complex parameter with the dimensions of length. The limiting cases of a free surface and an inextensible film correspond, respectively, to the limits $l_S/l_\nu\uparrow\infty$ and $l_S/l_\nu\downarrow 0$. We consider only these two cases in the interpretation of our experiments and refer to the corresponding surfaces as 'clean' or 'fully contaminated'. We remark that, in the general case (see the Appendix), l_S must be expected to depend on the frequency for harmonic motion (for which $\boldsymbol{u}$ and w may be regarded as complex amplitudes).

Capillary hysteresis is confined to a boundary layer that moves with the contact line C and has a lateral thickness of the order of the capillary length

$$l_c\equiv(T/g)^{1/2} \tag{1.3}$$

(T = kinematic surface tension, g = gravity), which is 2.7 mm for clean water. It often (especially for a hydrophobic container) dominates, and is less well understood than, wall and surface damping at laboratory scales. The hypothesis that the motion of C is resisted by a force proportional to its velocity, which is suggested (Miles 1967) by Ablett's (1923) measurements for small velocities, leads to the phenomenological condition (Hocking 1987; Miles 1991*a*)

$$c\boldsymbol{n}\cdot\boldsymbol{\nabla}\zeta=\partial_t\zeta, \tag{1.4}$$

where $\boldsymbol{n}$ is the inwardly directed normal to the lateral boundary, ζ is the surface displacement, and c is a parameter with the dimensions of velocity. But $\boldsymbol{\nabla}\zeta$ need not be in phase with $\partial_t\zeta$ in the frequency domain of interest, and c is expected to be complex for a monochromatic wave of complex amplitude ζ, for which $\partial_t\zeta=\mathrm{i}\omega\zeta$. (The available measurements, such as those of Ablett (1923), are for either very low frequencies or uniform translation, for which c is real.) The limiting cases of free and fixed contact lines, for which (1.4) reduces to $\boldsymbol{n}\cdot\boldsymbol{\nabla}\zeta=0$ and $\zeta=0$, respectively, correspond to the limits $\gamma\rightarrow\infty$ and $\gamma\rightarrow 0$, where

$$\gamma\equiv c/\omega l_c. \tag{1.5}$$

The former condition, which is implicit in most of the literature of water-wave motion, is realized for long gravity waves but not at centimetre scales. The latter condition is realized in a brimfull, sharp-edged container, as in the seminal experiments of Benjamin & Scott (1979).

Of the various sources of damping enumerated in the opening paragraph, only Stokes-boundary-layer and interior damping are amenable to calculation from first principles. Experimental confirmation of such calculations has been hampered by uncertainties associated with the remaining sources, especially the contact line and surface film; conversely, accurate determinations of contact-line and surface-film damping requires the accurate determination of Stokes-boundary-layer damping. We therefore undertook a theoretical and experimental study of waves in a deep, brimfull, circular cylinder of radius a and depth d for which

$$l_\nu<l_c\ll a, \tag{1.6}$$

and either $l_S \gg l_\nu$ (clean surface) or $l_S \ll l_\nu$ (fully contaminated surface). The restrictions $l_\nu/a \ll 1$ and $l_c/a \ll 1$ ensure that dissipation is confined to boundary layers. The choice of a circular cylinder eliminates possible difficulties with corners in the lateral boundary. The restriction to deep water reduces the number of parameters and eliminates possible difficulties with the flow at the intersection of the lateral and bottom boundaries (although this is a stagnation-point flow and therefore unlikely to be important for any configuration for which $d \gg l_\nu$). The brimfull condition presumably eliminates capillary hysteresis. The attainment of a clean surface eliminates surface-film damping (or, more precisely, renders it of higher order than Stokes-boundary-layer damping), while the attainment of a fully contaminated surface renders the surface-film boundary layer equivalent to a Stokes boundary layer.

We proceed as follows. In §2, we formulate and solve the eigenvalue problem for inviscid gravity–capillary waves in a circular cylinder with a fixed contact line. This problem was originally solved by Graham-Eagle (1983); however, the present solution is simpler and yields an eigenvalue equation that provides a more rapidly converging numerical solution *vis-à-vis* that of Graham-Eagle. In §3, we calculate the dissipation in the Stokes boundary layers on the lateral wall, the bottom and beneath a hypothetical surface film and then simplify the results by invoking $d/a \gg 1$. We describe the experimental apparatus and procedure in §4 and our results in §5. The surface-film problem for arbitrary l_S is solved in the Appendix.

2. The inviscid problem

The linear eigenvalue problem for inviscid gravity–capillary waves with a fixed contact line in a circular cylinder of radius a and depth d is prescribed by

$$\nabla^2\phi = 0 \quad (0 \leqslant r < a, -d < z < \zeta), \tag{2.1}$$

$$\partial_r\phi = 0 \quad (r = a), \quad \partial_z\phi = 0 \quad (z = -d), \quad \zeta = 0 \quad (r = a, z = 0), \tag{2.2a–c}$$

$$\partial_z\phi = \mathrm{i}\omega\zeta, \quad T\nabla^2\zeta - g\zeta = \mathrm{i}\omega\phi \quad (z = 0), \tag{2.3a, b}$$

where ϕ and ζ are the complex velocity potential and free-surface displacement, both of which comprise the implicit factor $\exp(\mathrm{i}\omega t)$, r, θ and z are cylindrical polar coordinates, $0 \leqslant \theta < 2\pi$, T is the kinematic surface tension, and the admissible values of the frequency ω (the *natural* frequencies) are to be determined.

We pose the solution of (2.1) and (2.2*a*, *b*) in the form

$$\phi = \phi_n(t)\, R_n(r) \cos s\theta \frac{\cosh k_n(z+d)}{\cosh k_n d}, \tag{2.4}$$

where

$$R_n(r) = \frac{J_s(k_n r)}{J_s(k_n a)}, \quad J_s'(\kappa_n) = 0, \quad \kappa_n \equiv k_n a, \tag{2.5a–c}$$

s is the azimuthal wavenumber, J_s is a Bessel function, and, here and subsequently, repeated indices are summed over the complete, orthogonal set $\{R_n, k_n\}$ except where the index occurs once but is not repeated on one side of an equation. Note that R_n and κ_n depend on s and that $\{1, 0\}$ is a non-trivial member of $\{R_n, k_n\}$ if and only if $s = 0$. Substituting (2.4) into (2.3*a*), we obtain the corresponding representation

$$\zeta = \zeta_n(t)\, R_n(r) \cos s\theta, \quad \zeta_n = (\mathrm{i}\omega)^{-1} \phi_n k_n T_n, \quad T_n \equiv \tanh k_n d. \tag{2.6a–c}$$

We obtain an alternative representation of ζ through the substitution of (2.4) into (2.3*b*), which yields

$$T\nabla^2\zeta - g\zeta = \mathrm{i}\omega\phi_n(t)\, R_n(r)\cos s\theta. \tag{2.7}$$

Separating the solution of (2.7) into a particular solution that describes the response of the free surface to the hydrodynamic pressure $-\rho\,\partial_t\,\phi$ and a complementary solution that satisfies the homogeneous capillary equation and is determined by the contact-line constraint (2.2*c*), we obtain

$$\zeta = A_n\, R_n(r)\cos s\theta - AC(r)\cos s\theta, \tag{2.8}$$

where

$$C(r) = \frac{I_s(r/l_c)}{I_s(a/l_c)}, \quad l_c \equiv \left(\frac{T}{g}\right)^{1/2}, \tag{2.9a, b}$$

I_s is a modified Bessel function, l_c is the capillary length,

$$A_n = \frac{-\mathrm{i}\omega\phi_n}{g + Tk_n^2}, \quad A = \sum_n A_n. \tag{2.10a, b}$$

Recasting (2.6*b*) and (2.10*a*) in the form

$$\phi_n = \mathrm{i}(\omega k_n\, T_n)^{-1}\,\omega_n^2\, A_n, \quad \zeta_n = (\omega_n/\omega)^2\, A_n, \tag{2.11a, b}$$

where

$$\omega_n \equiv [(g/a)\,\kappa_n\, T_n(1 + \kappa_n^2\,\lambda^2)]^{1/2} \tag{2.12}$$

is the nth natural frequency in the absence of the contact-line constraint (2.2*c*), substituting (2.11*b*) into (2.6*a*), and equating the result to (2.8), we obtain the compatibility condition

$$(\omega_n/\omega)^2\, A_n\, R_n(r) = A_n\, R_n(r) - AC(r). \tag{2.13}$$

It then follows from the Fourier–Bessel expansion

$$C(r) = C_n\, R_n(r), \tag{2.14}$$

where

$$C_n = \frac{\int_0^a CR_n\, r\,\mathrm{d}r}{\int_0^a R_n^2\, r\,\mathrm{d}r} = \left(\frac{2\lambda}{1+\kappa_n^2\,\lambda^2}\right)\left[\frac{I_s'(1/\lambda)}{I_s(1/\lambda)}\right]\left(\frac{\kappa_n^2}{\kappa_n^2 - s^2}\right) \quad \left(\lambda \equiv \frac{l_c}{a}, \kappa_n \equiv k_n\, a\right), \tag{2.15}$$

and the orthogonality of the $R_n(r)$ that

$$A_n = AC_n\left(\frac{\omega^2}{\omega^2 - \omega_n^2}\right). \tag{2.16}$$

Finally, we sum (2.16) over n and invoke (2.10*b*) to obtain (on the assumption that $A \neq 0$) the eigenvalue equation

$$C_n\left(\frac{\omega^2}{\omega^2 - \omega_n^2}\right) = 1 \tag{2.17}$$

for the determination of ω. We remark that (since the κ_n are prescribed by (2.5*b*)) C_n depends only on the capillary parameter λ and that the depth enters the eigenvalue

problem only through the ω_n. The roots of (2.17) may be determined by Newton's method. They evidently tend to $\{\omega_n\}$ as $\lambda \to 0$, in which limit $C_n = O(\lambda)$ and

$$\frac{\omega^2}{\omega_n^2} = 1 + \frac{2\lambda\kappa_n^2}{\kappa_n^2 - s^2} + O(\lambda^2). \tag{2.18}$$

The corresponding distribution of the ϕ_m, as determined by (2.11*a*) and (2.16) in the limit $\lambda \to 0$, $\omega \to \omega_n$, is given by

$$\frac{\phi_m}{\phi_n} = \left(\frac{2\lambda\kappa_m^2}{\kappa_m^2 - s^2}\right)\left(\frac{\omega_n^2}{\omega_n^2 - \omega_m^2}\right) + O(\lambda^2) \quad (m \neq n). \tag{2.19}$$

The approximations (2.18) and (2.19) are equivalent to those obtained on the assumption that capillary effects are confined to an $O(l_c)$ boundary layer (Miles 1991*a*).

An equivalent form of (2.17), which follows from the identity $\sum_n C_n = 1$ ($r = a$ in (2.14)) and reduces to that of Graham-Eagle (1983) for $d = \infty$ and $s = 0$, is

$$C_n\left(\frac{\omega_n^2}{\omega^2 - \omega_n^2}\right) = 0, \tag{2.20}$$

but it converges more slowly than (2.17).

3. Stokes boundary layers

The flow in a Stokes boundary layer is governed by the diffusion equation

$$\mathrm{i}\omega \boldsymbol{u} = \nu \boldsymbol{u}_{zz} \quad (z \geqslant 0), \tag{3.1}$$

where $\boldsymbol{u}$ is the tangential velocity, the time dependence $\exp(\mathrm{i}\omega t)$ is implicit, and z is the normal coordinate. The solution of (3.1), subject to the boundary conditions

$$\boldsymbol{u} = 0 \quad (z = 0), \quad \boldsymbol{u} \sim \boldsymbol{u}_o \quad (z/l_\nu \uparrow \infty), \tag{3.2a, b}$$

where $\boldsymbol{u}_o$ is the velocity at the outer edge of the boundary layer, is

$$\boldsymbol{u} = \boldsymbol{u}_o\{1 - \exp[-(\mathrm{i}\omega/\nu)^{1/2} z]\} \quad (\mathrm{i}^{1/2} = (1+\mathrm{i})/\sqrt{2}). \tag{3.3}$$

The resulting shear stress at the boundary is

$$\boldsymbol{\tau} = \rho\nu\,\partial_z \boldsymbol{u} = (1+\mathrm{i})\,\rho(\tfrac{1}{2}\nu\omega)^{1/2}\boldsymbol{u}_o, \tag{3.4}$$

from which it follows that the boundary-layer-induced perturbations of the real and imaginary parts of the natural frequency are equal; accordingly, the perturbed frequency has the form

$$\omega = \omega_0[1 - (1-\mathrm{i})\,\delta], \tag{3.5}$$

where ω_0 is the inviscid frequency and δ is the damping ratio.

If, as we assume, δ is small it is expedient to determine it through an energy calculation (cf. Miles 1967) according to

$$\delta = \frac{D}{2\omega E} \equiv \frac{1}{4}\left(\frac{l_\nu}{a}\right)\Delta, \quad l_\nu \equiv \left(\frac{2\nu}{\omega}\right)^{1/2}, \tag{3.6a, b}$$

where, from (3.2) and (3.4),

$$D = \tfrac{1}{2}\mathrm{Re}\iint \boldsymbol{\tau}\cdot\bar{\boldsymbol{u}}_o\,\mathrm{d}B = \tfrac{1}{2}\rho(\tfrac{1}{2}\nu\omega)^{1/2}\iint |\boldsymbol{u}_o|^2\,\mathrm{d}B, \tag{3.7}$$

is the mean dissipation rate, $\bar{\boldsymbol{u}}_o$ is the complex conjugate of $\boldsymbol{u}_o = \boldsymbol{\nabla}\phi$, $\mathrm{d}B$ is an element of the rigid boundary, which comprises the bottom ($z = -d$) and the lateral boundary ($r = a$) in the present application,

$$E = \tfrac{1}{2}\rho \iiint |\boldsymbol{\nabla}\phi|^2 \,\mathrm{d}V = \tfrac{1}{2}\rho \iint \phi\, \partial_z \bar{\phi}\, \mathrm{d}S \tag{3.8}$$

is the mean energy (twice the mean kinetic energy for a free oscillation) in the inviscid approximation, and S is the upper surface.

Substituting (2.4) into (3.7) (where $\boldsymbol{u}_o = \boldsymbol{\nabla}\phi$) and (3.8) and combining the results in (3.6a), we obtain

$$\Delta = \frac{\left[\delta_{mn}(\kappa_n^2 - s^2)(1 - T_n^2) + (\kappa_m \kappa_n + s^2)\left(\dfrac{T_m + T_n}{\kappa_m + \kappa_n}\right) - (\kappa_m \kappa_n - s^2)\left(\dfrac{T_m - T_n}{\kappa_m - \kappa_n}\right)\right]\phi_m \bar{\phi}_n}{(\kappa_l^2 - s^2)\,\kappa_l^{-1}\, T_l \phi_l \bar{\phi}_l}. \tag{3.9}$$

The first product in the numerator of (3.9) represents the bottom dissipation; the second and third products represent the sidewall dissipation. Letting $T_n = 1$, we obtain the deep-water approximation

$$\Delta = \frac{2(\kappa_m \kappa_n + s^2)(\kappa_m + \kappa_n)^{-1}\phi_m \bar{\phi}_n}{(\kappa_l^2 - s^2)\,\kappa_l^{-1}\phi_l \bar{\phi}_l}. \tag{3.10}$$

The further assumption that $\lambda \ll 1$ and the corresponding approximations (2.18) and (2.19) yield

$$\Delta = \left(\frac{\kappa_n^2 + s^2}{\kappa_n^2 - s^2}\right) + \frac{8\lambda \kappa_m^2 \kappa_n (\kappa_m \kappa_n + s^2)}{(\kappa_m + \kappa_n)(\kappa_m^2 - s^2)(\kappa_n^2 - s^2)}\left(\frac{\omega_n^2}{\omega_n^2 - \omega_m^2}\right) + O(\lambda^2), \tag{3.11}$$

in which n is not summed and $m = n$ is excluded from the summation over m.

The remaining (other than rigid-boundary) damping is negligible if the surface is clean. If, on the other hand, the surface is covered by an inextensible film, at which $\boldsymbol{u} = 0$, there is a Stokes boundary layer just below the film (where $\boldsymbol{u}_o$ is the tangential component of $\boldsymbol{\nabla}\phi$), which contributes

$$\Delta_S = \frac{(\kappa_n^2 - s^2)\,\phi_n \bar{\phi}_n}{(\kappa_l^2 - s^2)\,\kappa_l^{-1}\, T_l \phi_l \bar{\phi}_l} \tag{3.12}$$

to Δ; accordingly, the factor $1 - T_n^2$ is replaced by $2 - T_n^2$ in the numerator of (3.9), $\delta_{mn}(\kappa_n^2 - s^2)$ must be added to the coefficient of $\phi_m \bar{\phi}_n$ in the numerator of (3.10), and κ_n must be added to the right-hand side of (3.11).

4. Experimental apparatus and procedure

We measured the natural frequencies and damping rates of the six lowest modes in a brimfull, right circular cylinder. The experimental apparatus comprised an acrylic circular cylinder, an electromagnetic shaker with feedback, water from two sources, and a non-intrusive wave gauge. The cylinder had a radius $a = 2.766 \pm 0.0005$ cm and depth $d = 3.80 \pm 0.005$ cm measured from the bottom to the brim of the cylinder, which was machined to have a sharp edge. We cleaned the cylinder prior to filling by soaking in Micro (brand) laboratory cleaner, a non-toxic, biodegradable alternative to

chromic acid that cleans plastics as well as glass. After soaking, we rinsed the cylinder in distilled water and vacuumed it dry.

We conducted three sets of experiments using two water sources. In the first two sets we used water that was distilled and filtered of particles greater than 2 μm through Whatman slow filter paper. The third set used HPLC (high-grade chromotography) water from Sigma Chemicals. A simple test for pure water is provided by rising bubbles (Scott 1979); if a bubble persists at the surface for as long as 0.5 s the water is considered to be contaminated. The distilled water failed this test; bubbles persisted about a second. The HPLC water passed this test; bubbles persisted for 0.09 s. (This measurement was obtained by creating bubbles with an intrusive pipette and observing them with a high-speed digital imaging system (Kodak Ektapro) operating at 500 frame s^{-1}.) But Kitchener & Cooper (1959) give a bubble-persistence time of 'roughly 0.01 s' for a clean surface, which suggests that even the HPLC surfaces may not have been adequately pure. In all of the experiments we over-filled the cylinder and then vacuumed the excess with a micro-pipette attached to a vacuum pump. The surface was determined to be flat by observation of a horizontal laser beam that was flush with the cylinder's brim. The meniscus of the over-full cylinder diffracted the beam into a vertical line on a white sheet behind the cylinder; this line contracted to a point when the water was flat. We also observed the reflection of a vertical metal rod in the water surface; the reflection appeared undistorted across the contact line when the surface was flat.

In the first set of experiments, referred to as *distilled-clean*, we excited the wave field, turned off the forcing, and measured a time series of the wave decay within the first minute after the surface had been cleaned. In the second set of experiments, referred to as *contaminated*, we measured the time series of the decaying wave field five minutes after the surface had been cleaned. We chose this time period, rather than a longer interval, to limit evaporation, which causes surface curvature. The results sometimes changed if we re-did the experiment after the five-minute period; however, the results were reproducible if the experiment was conducted within five minutes after the surface had been cleaned. In the third set of experiments, referred to as *HPLC-clean*, we measured the time series of the decaying wave field within a minute after cleaning; however, the results did not change over a three-hour period. The experimental apparatus was enclosed in an acrylic box (that was not temperature-controlled) for the HPLC-clean experiments, but was open to the ambient atmosphere in the distilled experiments.

A Bruel & Kjaer minishaker Type 4810 drove the cylinder vertically to excite waves at half the forcing frequency. A non-contacting position transducer (Kaman model KD-2310) monitored the shaker motion and provided a signal to a servo-controller to ensure proper motion. A Micro-VAX II workstation with analog-to-digital, digital-to-analog and two independent real-time clocks provided the forcing signals. The forcing frequency was accurate to within 10^{-6} Hz.

A non-intrusive Wayne-Kerr capacitance probe measured the surface displacement by measuring the field between the water surface and the probe. It averaged over the surface area of the probe, which had a circular cross-section with diameter of 0.25 in. The probe had to be within a few millimeters of the water surface to ensure linearity between surface displacement and output voltage; accordingly, the wave amplitudes were kept smaller than 2 mm. We filtered the gauge signal through a Krohn-Hite Model 3323 low-pass, analog filter, which also provided a 20 db gain, and digitized it with the computer at 350 Hz. The time series was complex-demodulated at half the forcing frequency to obtain the amplitude and phase of the wave as a function of time.

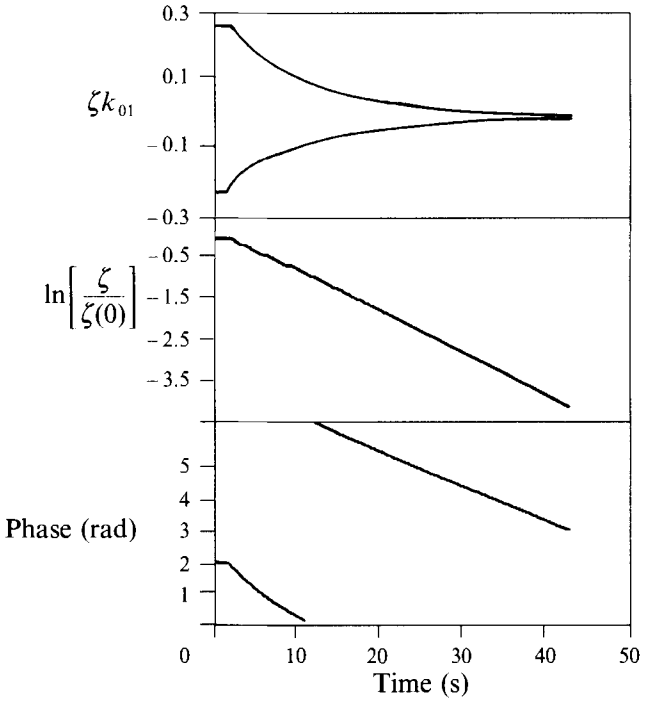

FIGURE 1. (*a*) Envelope of the time series of the wave slope, (*b*) natural log of the amplitude normalized by the steady-state amplitude, and (*c*) phase of a (0, 1) mode on clean (HPLC) water.

Figure 1 shows the envelope of the raw time series and the complex-demodulated amplitudes and phases from a typical experiment. The amplitude is shown on a (natural) log scale; thus the slope of the curve gives the dimensional damping rate, γ. The phase plot provides a measure of the natural frequency. The phase is constant if the wave frequency is equal to the frequency of complex-demodulation, while the slope of a linear variation in the phase corresponds to the difference between the actual wave frequency and the frequency of complex-demodulation. Thus, figure 1 (*c*) shows a line with zero slope initially, which corresponds to the wave with forcing present, and then a line with a non-zero slope, which corresponds to an unforced wave. Over this second portion of the phase–time curve, the wave is oscillating at its natural frequency. The slope of this line corresponds to the difference between the natural frequency and half the forcing frequency. Measurements of the natural frequency of the fundamental mode using this method were consistent with those obtained by measuring the resonance response of that mode to horizontal forcing. The wave excited by horizontal forcing attains its largest amplitude when the forcing frequency equals the natural frequency, which therefore provides a determination of the natural frequency. We also measured the neutral stability curves (to appear in a future paper) of most of the modes herein; the minima of these curves correspond to the natural frequencies of the modes and were consistent with values measured from the complex-demodulation procedure.

5. Results

We now discuss the measurements of natural frequency and damping rate for the lowest six modes in a circular cylinder. We compare the measurements with calculations that consider the surface to be either free (clean) or inextensible (fully contaminated).

			Measurements		Calculations				
					$f^{(2)} = \omega/2\pi$	$f^{(3)}$		$\dfrac{f^{(1)}}{f^{(3)}}$	$\dfrac{\Delta^{meas}}{\Delta^{calc}}$
(s,m)	κ_n	$\omega_n/2\pi$	$f^{(1)}$	Δ	inviscid (2.17)	viscous correction	Δ		
(1,0)	1.841	4.105	4.65	1.4	4.677	4.66	1.13	1.00	1.2
(2,0)	3.054	5.465	6.32	1.8	6.353	6.32	1.24	1.00	1.4
(0,1)	3.832	6.266	6.84	1.2	6.753	6.73	0.44	1.02	2.7
(3,0)	4.201	6.642	7.80	2.2	7.836	7.79	1.29	1.00	1.7
(4,0)	5.318	7.794	9.26	2.4	9.289	9.24	1.32	1.00	1.8
(1,1)	5.331	7.809	8.57	1.5	8.597	8.57	0.48	1.00	3.1

TABLE 1. Measured and predicted natural frequencies f (in c.p.s.) and non-dimensional damping rates Δ of the (s,m) mode with s nodal diameters and m nodal circles on HPCL water for which the contact line was pinned and the surface was clean.

5.1. *Clean-surface results*

Table 1 shows the predictions and measurements of natural frequencies and damping rates for the HPLC-clean experiments. The nth mode with s nodal diameters and m nodal circles has a frequency ω_n from (2.12), with $T = 72.4$ dyn cm^{-1}, which corresponds to the natural frequency when the contact line is free. When the contact line is pinned, the natural frequency ω is obtained from (2.17). Viscous damping has a small effect on the natural frequencies. If it arises from Stokes-type boundary layers, we can incorporate the measured damping rates into the prediction according to $f^{(3)}_{sm} = f^{(2)}_{sm} - (\gamma_{sm}/2\pi)$ where γ_{sm} is the measured damping rate of the (s,m) mode. The ratios $f^{(1)}/f^{(3)}$ between the measured and viscous-corrected, predicted natural frequencies agree within experimental accuracy for all modes except the (0, 1) mode. (The ratios $f^{(1)}/f^{(2)}$, which compare the measured natural frequencies to the inviscid calculations are either 0.99 or 1.00 for all modes except the (0, 1) mode.) We do not know why the theory underpredicts the frequency of the (0, 1) mode. Previously published predictions of natural frequency agree well with our measured results. Graham-Eagle (1983) predicted a natural frequency $f_{01} = 6.874$ Hz for the (0, 1) mode, which is within 0.5% of the measured value. Miles (1991*a*) predicted a natural frequency of $f_{10} = 4.637$ Hz for the (1, 0) mode, which is within 0.3% of the measured value.

The (4, 0) and (1, 1) modes have approximately equal wavenumbers. When the contact line is free, the natural frequencies from (2.12) of these two modes are very close with $f_{11} > f_{40}$. However, when the contact line is pinned, both calculation and experiment imply $f_{11} < f_{40}$. Hence, for some contact-line condition between these two extremes the two modes must have the same natural frequencies. We observed the resonance associated with the proximity of these two frequencies for the free contact line, for which the difference is 0.2%, but not for the pinned contact line, for which the difference is 7.5%. In some experiments using the (2, 0) mode, a slight unsteadiness was apparent in the decaying time series. The unsteadiness appeared as a high-frequency modulation, similar to the high-frequency precession instability observed by Henderson & Miles (1991) in experiments on the internal resonance between a (0, 1) mode and its superharmonic, (0, 3) mode. No precession instability or resonance was visible to the eye, and the measurements were the same in experiments with time series that did not display the unsteadiness as in experiments with time series that did.

The measured and predicted damping rates do not agree satisfactorily, as shown by

the last column of table 1. The predicted values on a clean surface are given by (3.10), with the amplitudes of the velocity potentials calculated from (2.11*a*), (2.12), (2.15), and (2.17). We note that the theoretical results do not change within the accuracy of table 1 when the assumption of infinite depth used in (3.9) is relaxed. The predicted damping rates increase somewhat, particularly for the higher modes, under the assumptions that produce (3.11); but the somewhat better agreement with measurements using (3.11) is due to these assumptions, and we have tabulated the calculations from (3.10). The measured values, Δ, are obtained by normalizing the measured (dimensional) damping rate, γ, through (3.6), where δ is the ratio of actual to critical damping; hence, $\Delta = 4a\gamma/(2\nu\omega)^{1/2}$, where $a = 2.766$ cm is the cylinder radius, $\nu = 0.01$ cm^2 s^{-1} is the kinematic viscosity, and ω is calculated from (2.17) and tabulated in column 6 of table 1.

The cause of the large discrepancies between predicted and measured damping is unknown. The results did not change when we conducted experiments in which the cylinder was pushed out-of-level a small amount. Nor did they change with the placement of the wave gauge (so that the fact that the gauge averaged over a small portion of the surface area was not a significant factor). Finally, the results did not change when we conducted experiments over a three-hour period, during which a small amount of fluid evaporated, causing a slight curvature at the endwalls; accordingly, a slight curvature was not significant in the experiments. Moreover, the reproducibility over this long period indicates that the hood enclosing the experiments was adequate in preventing contamination of the surface from the atmosphere. We also infer from this reproducibility that there were no contaminants from the water's interior that could rise to the surface and cause a variation in results between those obtained immediately, and those obtained sometime after cleaning the surface. Hence, we feel that the surface contamination was minimal. However, we note that the discrepancy between theory and experiment increased with increasing wavenumber. This result is consistent with the supposition that surface contamination caused the discrepancies, since surface contamination presumably becomes more effective in damping waves as the wavelength decreases toward the capillary length. It is possible that the surface contamination implied by bubbles popping in 0.09 s rather than 'roughly 0.01 s' could have caused the large discrepancies between predictions and measurements; however, for the reasons discussed below, we regard this as unlikely.

Henderson *et al.* (1992) measured damping rates for the (0, 1) mode with a free contact line that were 1.2 times larger than predictions from the free-end, clean-surface theory when the static contact angle was $\geqslant 90°$ and 1.5 times larger than predictions from the free-end, clean-surface theory when the static contact angle was $< 90°$. They used a cylinder with the same radius as in the present (above) experiments and water of depth 2.00 cm that was doubly distilled and filtered of particles up to 11 μm. They cleaned the surface in the same manner as described herein and attributed the discrepancies between measurements and predictions to contact-line effects. Possible losses of energy due to contact-angle hysteresis, waves formed by meniscus oscillations, and the curvature due to the meniscus are absent in the present experiments, for which the contact line was pinned and the surface was flat. In addition, the experiments of Henderson *et al.* were open to the atmosphere and used an *in-situ* wave gauge that increases damping a small amount; hence, the techniques used herein are more satisfactory than theirs, and we would expect better agreement between theory and experiment for the pinned-contact-line experiments.

Case & Parkinson (1957) report measurements of the damping rate of the (1, 0) mode with a free contact line in a polished brass cylinder that were in agreement with the

(s,m)	f	Δ	$\frac{\Delta^{meas}}{\Delta^{calc}}$
(1,0)	4.65	1.4	1.2
(2,0)	6.32	2.2	1.8
(0,1)	6.83	1.8	4.1
(3,0)	7.79	2.7	2.1
(4,0)	9.24	2.9	2.2
(1,1)	8.57	2.1	4.4

TABLE 2. Measured natural frequencies f (in c.p.s.) and non-dimensional damping rates Δ of the (s, m) mode with s nodal diameters and m nodal circles on filtered, distilled water for which the contact line was pinned and the surface was cleaned.

clean-surface, predicted value. We find this agreement surprising in that Case & Parkinson used tap water, which is known to increase damping rates significantly over the clean-surface value, and an *in-situ* probe, which increases damping rates a slight amount (or more, depending on the degree of care taken). We therefore tried duplicating their results with the techniques described above for the HPLC-clean experiments and a polished brass cylinder of radius 3.181 cm. Our measured damping rates were 1.12 times larger than the predicted values.

We also measured damping rates and natural frequencies using filtered, distilled water as described in §4. Table 2 shows that the natural frequencies were slightly smaller than those in the HPLC-clean experiments for three modes, while the damping rates were significantly larger for all modes except the fundamental sloshing mode. Presumably the HPLC experiments differed from the distilled-clean experiments owing to the presence of contaminants from both the interior and the atmosphere in the latter. If so, these results show that the natural frequencies are fairly insensitive to such perturbations, while the damping rates are extremely sensitive to surface contamination that arises either from the atmosphere or the water. As in the HPLC experiments, the discrepancy between theory and experiment is largest for the higher modes, for which surface contamination is expected to be more significant. Since the improvement associated with the replacement of distilled, filtered water with vacuumed surfaces by HPLC water was significant, it is possible that further improvement could be gained over the HPLC experiments. However, the results in both the HPLC-clean and distilled-clean experiments show that the discrepancy between theory and measurement is significantly larger for the modes with a nodal circle (the 0, 1 and 1, 1 modes) than for modes without nodal circles. We have no explanation for this effect of modal structure. The distilled-clean measurements were obtained within the first minute after the surface was clean. After that time the results changed dramatically as described in §5.2.

5.2. *Contaminated-surface results*

Table 3 shows measured and predicted natural frequencies and damping rates for pinned-edge waves on a contaminated surface. The measured natural frequencies, $f^{(4)}$, are less than those of waves on a clean surface. This decrease is due both to the enhanced viscous damping and to the decrease in surface tension that result from a contaminated surface. To obtain an estimate of the surface tension of the contaminated surface, we calculated an imputed, inviscid frequency $f^{(5)}_{sm} = f^{(4)}_{sm} + (\gamma_{sm}/2\pi)$ using the actual measured frequency $f^{(4)}_{sm}$ and the measured damping rate γ_{sm}. These imputed frequencies agree best with the inviscid calculations, $f^{(6)}$, from (2.17) for a surface

	Measurements			Calculations with $T = 66$ dyn cm^{-1}		
(s,m)	$f^{(4)}$	$f^{(5)}$ corrected for viscosity	Δ	$f^{(6)}$ (2.17)	Δ (3.8)	$\frac{\Delta}{\Delta^{calc}}$
(1,0)	4.63	4.69	5.8	4.64	3.19	1.8
(2,0)	6.19	6.29	7.7	6.29	4.70	1.6
(0,1)	6.68	6.77	7.2	6.70	4.45	1.6
(3,0)	7.62	7.73	8.1	7.73	6.06	1.3
(4,0)	8.96	9.10	9.4	9.13	7.34	1.3
(1,1)	8.37	8.49	8.9	8.49	6.12	1.4

TABLE 3. Measured and predicted natural frequencies f (in c.p.s.) and non-dimensional damping rates Δ of the (s,m) mode with s nodal diameters and m nodal circles on filtered, distilled water for which the contact line was pinned and the surface was contaminated. $f^{(4)}$ is the measured natural frequency; $f^{(5)}$ is the measured natural frequency corrected by the measured (dimensional) damping rate γ. Δ is the measured damping rate normalized by the predicted natural frequency $f^{(6)}$.

tension $T = 66$ dyn cm^{-1}. Using this value of surface tension, we calculated the damping rates Δ (in column 6) from (3.10) and (3.12) with (2.11a), (2.12), (2.15), and (2.17). The measured values of Δ (in column 4) were obtained by normalizing the measured damping rates as described in §5.1 with $\omega = 2\pi f^{(6)}$.

The measured damping rates of the waves on a contaminated surface are much greater than predicted by the theory that considers the surface to be an inextensible film. The discrepancy may be due to elasticity in the surface film, which can enhance damping ratios by a factor of two over the rates for an inextensible surface (see Miles 1967, figure 1). However, discrepancies due to surface films should dominate the higher modes for which wavelengths become comparable with the capillary length. Instead, table 3 shows that when surface contamination is considered the discrepancy between measurements and predictions is largest for the lower modes. The decrease in discrepancy between theory and experiment with increasing wavenumber suggests that surface contamination, as evidenced by either an inextensible or an elastic film, was not the primary cause of the discrepancy, but we do not have an alternative suggestion. We also note that the discrepancy between theory and experiment for modes with nodal circles was not significantly different from those without nodal circles in the contaminated experiments, while it was markedly different in the HPLC- and distilled-clean experiments.

6. Discussion

The theory satisfactorily predicts the natural frequencies of standing waves on a surface for which the contact line is pinned and the surface is clean. This agreement is much more consistent than for standing waves on a surface for which the contact line is free. For example, Henderson *et al.* (1992) showed that the natural frequency depends significantly on the static contact angle. Hence, the pinned-edge system is a good one to use if accuracy in predicting the natural frequencies is required for tuning possible nonlinear responses.

The theory is inadequate for the prediction of the measured damping rates of the waves on a surface for which the contact line was pinned. There is evidence that the discrepancies between theory and the clean-surface experiments were due to surface

effects. The discrepancy between theory and measurements increased with increasing wavenumber in accordance with the supposition that surface contamination has a larger effect on the higher modes. Moreover, as greater care was taken to achieve a clean surface, the damping rates decreased. Bubbles burst in 0.09 s at the surface of the HPLC water, indicating that some contamination might be present. Nevertheless, there is also evidence that surface effects were not the major cause of the discrepancy between theory and clean-surface experiments. Measurements using the HPLC water were reproducible from within the first minute of cleaning the surface to over a three-hour period, indicating that the procedures were adequate in minimizing surface contamination. Measurements (see §5.1) of damping rates for the (1, 0) and (0, 1) modes with a free contact line were better predicted by the free contact-line theory than measurements of the pinned-edge (1, 0) and (0, 1) modes by the pinned-edge theory. Presumably, the discrepancy between theory and experiment for the free-end mode was caused by contact-line dynamics, which were not present in the pinned-edge case. The water and water surfaces of the previous experiments were prepared the same as, or less satisfactorily than in the present experiments; accordingly, we would expect at least as good agreement as in the previous experiments. The discrepancy between theory and experiments for the modes with nodal circles was significantly larger than for modes with no nodal circles in the clean-surface experiments, suggesting some dependence of damping rate on modal structure. The discrepancy between (the inextensible surface) theory and contaminated-surface experiments decreased with increasing wavenumber, suggesting that surface films were not the dominant cause of disagreement when surface contamination was present in both the experiments and the theory.

Despite the large damping rates in comparison with predictions, the pinned-edge waves are advantageous if one is interested primarily in studying waves with a minimal damping rate. A comparison of the present results with those of Henderson *et al.* (1992) shows that, irregardless of theoretical predictions, the pinned-edge (clean-surface) waves damped with rates that were about 0.7 times those of the free-end waves for which the static contact angle was $\geqslant 90°$ and 0.5 times those of the free-end waves for which the static contact angle was $< 90°$.

This work was supported by the National Science Foundation through NSF Grants OCE92-16397 and DMS92-57456, by the Office of Naval Research N00014-92-J-1171, and by a fellowship (for D.M.H.) from the David & Lucille Packard Foundation.

Appendix. The surface-film problem

We seek the solution of the linearized Navier–Stokes and continuity equations

$$\partial_t \boldsymbol{q} = -\boldsymbol{\nabla}(p/\rho)+\nu\nabla^2\boldsymbol{q}, \quad \boldsymbol{\nabla}\cdot\boldsymbol{q} = 0 \quad (0 \leqslant r < a, 0 \leqslant \theta < 2\pi, -d < z < 0), \tag{A 1a, b}$$

subject to the boundary conditions

$$u = 0 \quad (r = a), \quad w = 0 \quad (z = -d), \quad \zeta = 0 \quad (r = a, z = 0), \tag{A 2a–c}$$

$$\partial_t \zeta = w, \quad T\nabla^2\zeta - g\zeta = -\frac{p}{\rho}+2\nu\partial_z w, \quad \boldsymbol{u}+l_S(\partial_z \boldsymbol{u}+\boldsymbol{\nabla}_2 w) = 0 \quad (z = 0), \tag{A 3a–c}$$

and the outer condition

$$\boldsymbol{q} \sim \boldsymbol{\nabla}\phi \quad (|z|/l_\nu \gg 1), \quad \phi = \phi_n(t)\, R_n(r)\cos s\theta \frac{\cosh k_n(z+d)}{\cosh k_n d}, \tag{A 4a, b}$$

where $\boldsymbol{q} \equiv (\boldsymbol{u}, w)$ is the particle velocity, $\boldsymbol{u}$, u and w are the horizontal, radial and vertical components thereof, p is the pressure, ζ is the surface displacement, T is the kinematic surface tension, l_S is a complex length, ∇_2 is the horizontal component of ∇, and ϕ is the inviscid solution of §2. We assume that both the viscous length l_ν (1.1) and the capillary length l_c (1.3) are small compared with a, by virtue of which the interaction of the surface-film and sidewall boundary layers may be neglected.

Following Miles (1991*b*), we pose the solution of (A 1)–(A 4) in the form

$$\boldsymbol{q} = \nabla\phi + \nabla \times (\nabla\chi \times \boldsymbol{z}_1), \quad p = -\rho\,\partial_t \phi, \tag{A 5a, b}$$

where $\nabla\chi \times \boldsymbol{z}_1$ is a vector potential and $\boldsymbol{z}_1$ is a vertical unit vector. Substituting (A 5) into (A 1), we obtain

$$\nabla^2\phi = 0, \quad \partial_t \chi = \nu\nabla^2\chi. \tag{A 6a, b}$$

The solution of (A 6), subject to (A 2a, b), is given by (A 4b) and the corresponding expansion

$$\chi = \chi_n(t)\, R_n(r) \cos s\theta\, \mathrm{e}^{\mu_n z}, \tag{A 7}$$

where, on the assumption of the harmonic time dependence $\exp(\mathrm{i}\omega t)$ and the invocation of $k_n l_\nu \ll 1$,

$$\mu_n = \left(\frac{\mathrm{i}\omega}{\nu} + k_n^2\right)^{1/2} \simeq \frac{1+\mathrm{i}}{l_\nu}. \tag{A 8}$$

Substituting

$$\boldsymbol{u} = (\phi_n + \mu_n \chi_n)\nabla[R_n(r)\cos s\theta], \quad w = (k_n T_n \phi_n + k_n^2 \chi_n) R_n(r)\cos s\theta \quad (z = 0) \tag{A 9a, b}$$

into (A 3c) and invoking the orthogonality of the $R_n(r)$, we obtain

$$\frac{\chi_n}{\phi_n} = -\left[\frac{1 + 2k_n T_n l_S}{\mu_n + l_S(\mu_n^2 + k_n^2)}\right] \simeq -\frac{l_\nu(1 + 2k_n T_n l_S)}{1 + \mathrm{i} + 2\mathrm{i}(l_S/l_\nu)} \quad (n \text{ not summed}). \tag{A 10}$$

Proceeding as in §2, we substitute (A 9b) into (A 3a, b) to obtain

$$\zeta = (\mathrm{i}\omega)^{-1}(k_n T_n \phi_n + k_n^2 \chi_n) R_n(r)\cos s\theta \tag{A 11a}$$

and

$$T\nabla^2\zeta - g\zeta = [\mathrm{i}\omega\phi_n + 2\nu k_n^2(\phi_n + \mu_n \chi_n)] R_n(r)\cos s\theta. \tag{A 11b}$$

Those may be solved as in §2 to obtain

$$C_n\left(\frac{\omega^2}{\omega^2 - \hat{\omega}_n^2}\right) = 1 \tag{A 12}$$

in place of (2.17), where C_n is given by (2.15), and

$$\hat{\omega}_n^2 = \omega_n^2\left[1 - \frac{k_n l_\nu(T_n^{-1} + 4k_n l_S)}{1 + \mathrm{i} + 2\mathrm{i}(l_S/l_\nu)}\right]. \tag{A 13}$$

The limit for an inextensible film yields the Stokes-boundary-layer result

$$\hat{\omega}_n^2 \sim \omega_n^2[1 - \tfrac{1}{2}(1 - \mathrm{i})\, k_n T_n^{-1} l_\nu] \quad (l_S/l_\nu \to 0). \tag{A 14}$$

The limit of a free surface yields

$$\tilde{\omega}_n^2 \sim \omega_n^2(1 - 2\mathrm{i}k_n^2 l_\nu^2) \quad (l_S/l_\nu \to \infty), \tag{A 15}$$

in which the viscous term is negligible compared with that for a Stokes boundary layer.

The parameter l_S/l_ν is positive-imaginary for gravity waves and an insoluble surface

film (Miles 1967, 1991*b*), and the contribution of surface-film damping to the damping ratio δ then varies from the asymptotic value $(k_n/T_n)l_v$ for $|l_S|/l_v \to 0$ through a maximum of twice the asymptotic value for $|l_S|/l_v = \frac{1}{2}$ to $k_n^2 l_v^2$ for $|l_S/l_v| \to \infty$.

REFERENCES

ABLETT, R. 1923 An investigation of the angle of contact between paraffin wax and water. *Phil. Mag.* **46**, 244–256.

BENJAMIN, T. B. & SCOTT, J. C. 1979 Gravity–capillary waves with edge constraints. *J. Fluid Mech.* **92**, 241–267.

CASE, K. M. & PARKINSON, W. C. 1957 Damping of surface waves in an incompressible liquid. *J. Fluid Mech.* **2**, 172–184.

DORE, B. D. 1978 Some effects of the air–water interface on gravity waves. *Geophys. Astrophys. Fluid Dyn.* **10**, 215–230.

GRAHAM-EAGLE, J. 1983 A new method for calculating eigenvalues with applications to gravity–capillary waves with edge constraints. *Math. Proc. Camb. Phil. Soc.* **94**, 553–564.

HENDERSON, D. M., HAMMACK, J., KUMAR, P. & SHAH, D. 1992 The effects of static contact angles on standing waves. *Phys. Fluids* A **4**, 2320–2322.

HENDERSON, D. M. & MILES, J. W. 1991 Faraday waves in 2:1 internal resonance. *J. Fluid Mech.* **222**, 429–470.

HOCKING, L. M. 1987 The damping of capillary gravity waves at a rigid boundary. *J. Fluid Mech.* **179**, 253–256.

KITCHENER, J. A. & COOPER, C. F. 1959 Current concepts in the theory of foaming. *Q. Rev. Chem. Soc.* **13**, 71–97.

MILES, J. W. 1967 Surface-wave damping in closed basins. *Proc. R. Soc. Lond.* A **297**, 459–473.

MILES, J. 1991*a* The capillary boundary layer for standing waves. *J. Fluid Mech.* **222**, 197–205.

MILES, J. 1991*b* A note on surface films and surface waves. *Wave Motion* **13**, 303–306.

SCOTT, J. C. 1977 The historical development of wave-calming using oil. *Rep.* 81. Fluid Mechanics Research Institute, University of Essex.

SCOTT, J. C. 1979 The preparation of clean water surfaces for fluid mechanics. In *Surface Contamination: Genesis, Detection and Control*, vol. 1 (ed. K. L. Mittal), pp. 477–497. Plenum.

STOKES, C. G. 1851 On the effect of the internal friction of fluids on the motion of pendulums. *Trans. Camb. Phil. Soc.* **9**, 8–106 (also *Mathematical and Physical Papers*, vol. 3, pp. 1–141, Cambridge University Press, 1922).